Dynamic Features of Transition States for β-Scission Reactions of Alkenes over Acid Zeolites Revealed by AIMD Simulations

Jérôme Rey, Charles Bignaud, Pascal Raybaud, Tomáš Bučko, Céline Chizallet

Dynamic features of transition states for β-scission reactions of alkenes over acid zeolites revealed by AIMD simulations

Jérôme Rey,[a] Charles Bignaud,[a,b] Pascal Raybaud,[a] Tomáš Bučko*[c], Céline Chizallet*[a]

[a] Dr. J. Rey, C. Bignaud, Dr. P. Raybaud, Dr. C. Chizallet
IFP Energies nouvelles
Rond-Point de l'échangeur de Solaize, BP3, 69360 Solaize, France
E-mail: celine.chizallet@ifpen.fr
[b] C. Bignaud
Département de chimie, École normale supérieure, PSL University, 75005 Paris, France
[c] Dr. T. Bučko
Department of Physical and Theoretical Chemistry, Faculty of Natural Sciences, Comenius University in Bratislava, Ilkovičova 6, SK- 84215 Bratislava, Slovakia
Institute of Inorganic Chemistry, Slovak Academy of Sciences, Dúbravská cesta 9, SK-84236 Bratislava, Slovakia
E-mail: tomas.bucko@uniba.sk

Abstract:

Zeolite-catalyzed alkene cracking is key to optimize the size of hydrocarbons. The nature and stability of intermediates and transition states (TS) are, however, still debated. Herein, transition path sampling and blue moon ensemble density functional theory simulations are combined to unravel the behavior of C_7 alkenes in CHA zeolite. Free energy profiles are determined, linking π-complexes, alkoxides and carbenium ions, for B_1 (secondary to tertiary) and B_2 (tertiary to secondary) β-scissions. B_1 is found to be easier than B_2. The TS for B_1 occurs at the breaking of the C-C bond, while for B_2 it is the proton transfer from propenium to the zeolite. We highlight the dynamic behaviors of the various intermediates along both pathways, which reduce activation energies with respect to those previously evaluated by static approaches. We finally revisit the ranking of isomerization and cracking rate constants, which are crucial for future kinetic studies.

Zeolite-catalyzed cracking of alkenes is a long-debated reaction[1] that has prominent –positive or negative- impact in refining, petrochemistry, natural gas and biomass conversions.[2] It is generally assumed that cracking reactions proceed via sequence of steps involving protonation of the C=C bond by the zeolite's Brønsted site, β-scissions, and proton transfer back to the zeolite. Carbenium ions were invoked as intermediates.[3] β-scission mechanisms were classified according to the nature of the carbenium ions formed before and after cracking. Among these mechanisms, B_1 converts secondary carbenium ions into tertiary ones, whereas B_2 β-scission transforms tertiary carbenium ions into secondary ones (Scheme 1).[4] They play a very important role in the hydrocracking reaction network of hydrocarbons, in particular in large pore zeolites.[5] As they are taking place at the same time as alkene skeletal isomerization reactions, it is highly challenging to deduce intrinsic rate constants of elementary steps from experiments. Advanced kinetic models were proposed that accurately reproduced the observed isomerization and cracking selectivities in given operating condition windows.[6] However, building universal predictive models still represents a challenge that requires an in-depth knowledge of the intrinsic kinetic features of each kind of steps.

Density functional theory (DFT) calculations are powerful for the identification of relevant intermediates and transition states (TS), and for predictions of their stability. Until very recently, the theoretical determination of mechanisms of cracking of olefins and of the corresponding barriers was done in the framework of static DFT calculations. Most often, alkoxides instead of carbenium ions were considered as reactants and products, and thermal and entropic effects were neglected.[7] Large potential energy barriers were computed (often higher than 100 kJ/mol), with large variations from one study to the other, depending on the configuration chosen as a starting point. For acid-catalyzed reactions in zeolites, severe limitations of static calculations were identified recently, both in terms of chemical nature of intermediates and of free energy estimations. Advanced ab initio molecular dynamics (AIMD) is a relevant option,[8] although computationally highly demanding, that brought some unprecedented level of knowledge for alkene isomerization[9] and cracking.[10] Cnudde et al. found a free energy barrier for B_2 cracking of dibranched C_8 alkenes close to 70 kJ/mol at 773 K, lower than by static calculations (90 to 197 kJ/mol).[10] The B_1 reaction was assumed to play a minor role compared to B_2, and it was not considered in their study. In microkinetic modeling, B_1 and B_2 rate constants are often supposed to be equivalent.[6a] In the present work, we address explicitly the crucial question of the B_1 and B_2 β-scissions, so as to unravel the nature of relevant intermediates and TS, and to decipher their rate constant ranking. To this end, we rely on a set of advanced AIMD, considering chabazite as a model

large-cage zeolite (SI S1-4), with the cage size similar to that of Beta zeolite (used in practice for hydrocracking[11]), but with a more affordable computational cost. Alkene cracking in CHA also answers practical questions that are raised in the context of the Methanol-to-Olefin process.[2c] The simulation temperature of 500 K is considered throughout this work, being representative of working conditions of hydrocracking catalysts.[4 ,5a,5b ,6,11]

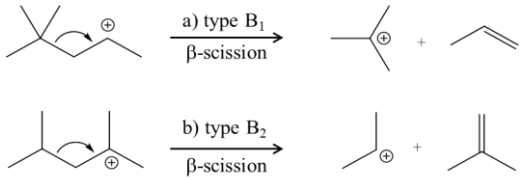

Scheme 1. β-scission mechanisms: a) type B_1 involving secondary 4,4-dimethyl-penten-2-ium to tertiary tert-butylium cations. b) type B_2 involving tertiary 2,4-dimethyl-penten-2-ium to secondary cations propenium cations .

First, the type B_1 β-scission of the 4,4-dimethyl-penten-2-ium dibranched secondary cation (I) is investigated (Scheme 1.a). Free MD runs starting from I in revealed that isomerization into a more stable tertiary dibranched reactant, the 2,3-dimethyl-penten-2-ium tertiary cation R, takes place. In order to identify the landscape of reactions, we employed the transition path sampling method[12] (TPS) (SI S3) that is best suited for this purpose. In this way, an ensemble of short trajectories linking R with I were generated. Subsequently, these trajectories were continued by straightforward MD in order to identify the stable products, given in Figure 1. Out of all trajectories leading to stable products, only 5.3 % resulted into direct cracking, while formation of alkoxide (4,4-dimethyl-pent-2-oxide) was observed in 15.3 % of cases, and 79.4 % of trajectories corresponded to one of three different π-complexes (namely 4,4-dimethyl-pent-1-ene (45.9%), (Z)- and (E)-4,4-dimethyl-pent-2-ene (1.5% and 52.6%, respectively)) formed with proton located on two distinct oxygen atoms next to Al (in 41% and 59% of the cases, respectively) giving rise to six different reactions for the formation of π-complexes.

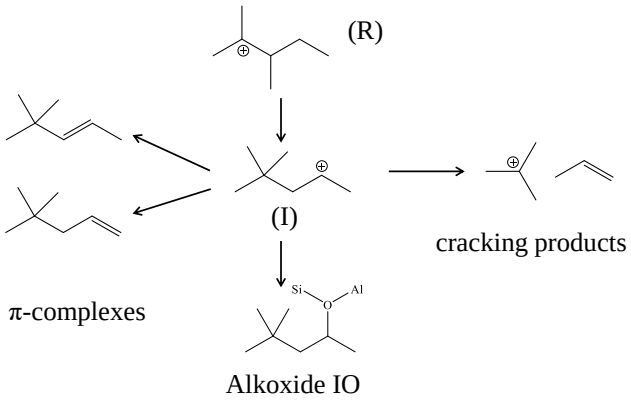

Figure 1. Reaction routes identified by transition path sampling at 500 K leading to different products connected to the B1 β-scission products.

Armed with this knowledge, accurate free energy profiles corresponding to the dominant reactions were determined by a set of blue moon sampling simulations (SI S4), considering the occurrence of the reactive rotamer of R among all rotamers (SI S6-7), and focusing on four key steps (Figure 2):

i) the R→I isomerization, involving methyl shift followed by hydride shift (SI S7). This is, however, not a two-step process, insofar as no reaction intermediate has been identified,

ii) the protonation of (E)-4,4-dimethyl-pent-2-ene (dominant π-complex in TPS) followed by carbenium β-scission (SI S8.1),

iii) the C-O bond breaking of 4,4-dimethyl-pent-2-oxide followed by carbenium β-scission (SI S8.2),

iv) the reaction connecting R to the π-complex (R→π), equivalent to a methyl shift plus proton shift from the carbenium to the zeolite network (SI S9). The TS of this last reaction corresponds to that of the proton transfer back to the zeolite.

The R→I isomerization by two successive type A isomerization reactions (a methyl shift followed by a hydride shift) is an activated process with a free energy barrier of 60.9 ± 3.8 kJ/mol, controlled by the hydride shift. It is slightly lower than that of a 1,3 hydride shift from a tertiary to a secondary carbenium ion as calculated in our previous work (67.4 kJ/mol at 500 K).[9a] Thus, these type A isomerization reactions have comparable kinetics and are faster than type B isomerizations,[9a] as expected empirically.[2a] The two type A isomerizations needed to connect R with I are consecutive rather than synchronous and, contrary to the general belief, no stable intermediate on the free energy surface exists between the two reaction steps. The TS is formed during the hydride shift. The secondary cation I, the precursor of cracking, is a very short-lived intermediate, which free energy can only be approximately estimated in Figure 2.

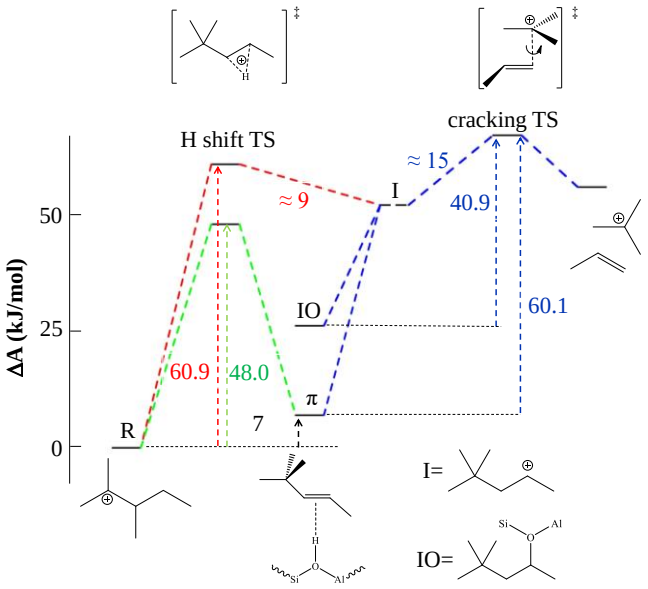

Figure 2. Overall free energy profile of the different routes involved in the type B_1 β-scission, investigated by blue moon sampling MD simulations at 500 K. A qualitative estimate of the free energy of the secondary cation 4,4-dimethyl-penten-2-ium (I) is indicated.

Indeed, the I cation undergoes spontaneous cracking or, with even higher likelihood, it can reform an alkoxide or several π-complexes. These latter ones can be subsequently cracked, with a free energy barrier of a similar magnitude as obtained for the isomerization of the R into I. The tertiary cation and the π-complexe are intermediates of similar stabilities, whereas the alkoxide (IO) is by 23.9 kJ/mol less stable than the π-complex. We built a kinetic model integrating the data displayed in Figure 2 (SI S10), showing that the cracking mechanism from the π-complex is strongly dominant over that from R (via I), that in turn preferentially transforms into the π-complex: the latter is the key reaction intermediate.

As already discussed, alkoxide was considered as the reactant in most of the previous static DFT studies.[7] We find here that the tertiary cation and π-complex are more relevant intermediates, being 26 and 19 kJ/mol lower in free energy than the alkoxide, respectively. The free energy barriers obtained for the type B_1 β-scission (60.1 ± 4.2 kJ/mol starting from the π-complex, 67.1 kJ/mol starting from the tertiary cation) are much lower than the energy barriers determined previously either by DFT static approach (significantly higher than 100 kJ/mol [7f,7h], starting most of time from alkoxides) or by kinetic modeling (~120 kJ/mol,[6b,6c] written from carbenium ions). However, these approaches provide only approximate activation entropies. As the forthcoming analysis will illustrate, our AIMD method does include unexpected structural behavior of the TS impacting entropic contributions. On the other hand, our free energy barriers are consistent with the ones obtained in biased MD for type A (53 kJ/mol) and B_2 (around 70 kJ/mol) β-scissions by Cnudde et al.[10]

B_1 cracking requires a specific conformation of the TS to occur, where the planes of the two hydrocarbon fragments are approximately parallel (Figure 3-a). The average distance C^2–C^3 between the two carbon atoms of the breaking bond is 2.19 Å in the simulations starting from the π-complex and 2.23 Å starting from the alkoxide (SI S11). The C^2-C^4 distance (2.64 Å on average) is longer than C^2-C^3, showing that the carbon atom C^2 (of the tert-butylium cation to be formed) interacts preferentially with the carbon atom C^3 of the double bond C^3-C^4 of the propene in formation. However, electron localization function analysis[13] demonstrates also that this interaction between the two fragments is not covalent, since no basin assignable to electron pairs is formed between the C^2 and C^3 atoms (Figure S19).

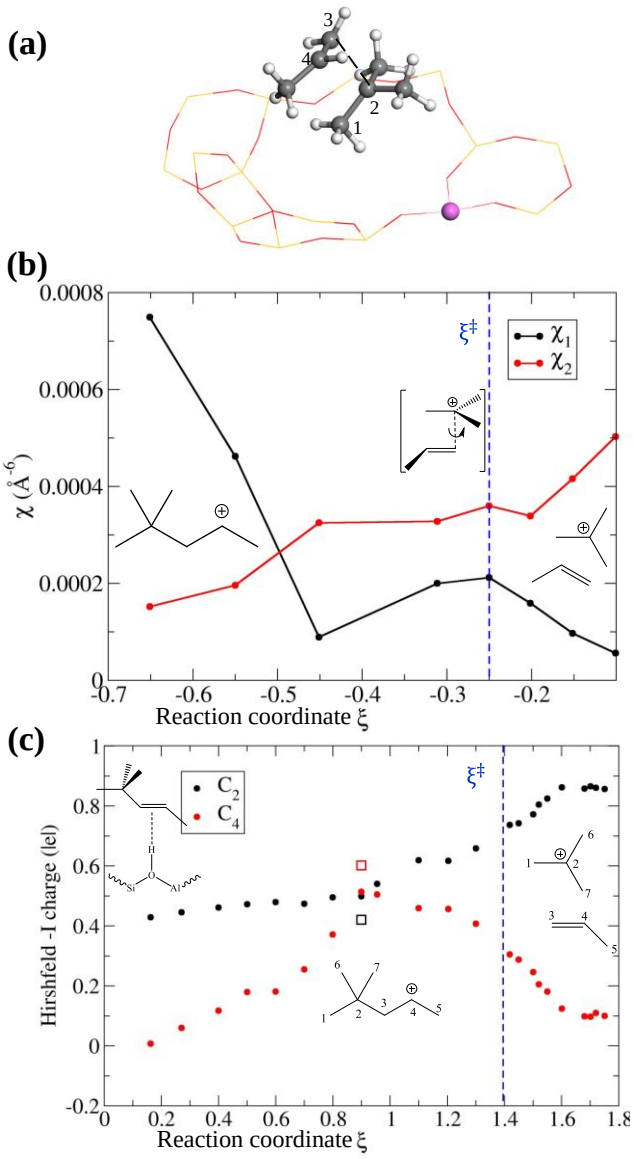

Figure 3. (a) Selected structure from the constrained MD simulation of the TS of the type B_1 cracking reaction starting from the π-complex (E)-4,4-dimethyl-pent-2-ene (Grey: C, white: H, purple: Al, red and yellow lines are broken at O and Si positions respectively). (b) Evolution of the χ parameters (defined via Equation (1)) as a function of ξ, for the type B_1 β-scission starting from an alkoxide. (c) Hirshfeld-I charges of selected carbon atoms of the C_7 species as a function of ξ for the cracking reaction starting from the π-complex. Charges for the corresponding gas phase optimized structures are reported with empty squares. All other carbon atoms have negative charges (around -0.5|e|).

Hence, this interaction (of electrostatic nature) allows a virtually free rotation of the two fragments with respect to each other, as shown by the wide distribution of the dihedral angle defined by the C^1-C^2-C^3-C^4 sequence (Figure S18). This internal rotational degree of freedom may explain the low free energy of activation obtained by AIMD in comparison with the activation energies reported by previous static or kinetic approaches. Moreover, a global rotation of the C_7 species is observed during the cracking reaction. This rotation features the exchange of the fragment facing the aluminum atom bearing the conjugated basic O-site of the acid zeolite: initially the propenium fragment and the tert-butylium fragment at the end. The average positions of these two products of cracking are measured via the parameter χ (χ_1 for propene, χ_2 for tert-butylium) which is the time average of the sum of inverse distance between the carbon and Al atoms raised to the power of six (Equation (1), Figure 3-b).

$$\chi = \left\langle \sum_i \frac{1}{R_{Al-C_i}^{\,6}} \right\rangle \qquad (1)$$

When the secondary cation I is formed, the propene part of the C_7 skeleton is located near the aluminium atom ($\chi_1 > \chi_2$). During the cracking reaction, this propene in formation moves away from the aluminium atom and the tert-butylium cation gets closer to it, ($\chi_1 < \chi_2$). In the large cavity of chabazite, this global rotation of the C_7 species is not hindered. It may be anticipated that the pore size of zeolites and the acid site location will impact this rotational degree of freedom and thus the cracking mechanism.

This global rotation is related to the change of the charge distribution of the atoms which has been computed by iterative Hirsheld charges[14] for different states (Figure 3-c). The C^2 atom appears to be positively charged already in the initial state (π-complex), contrary to C^4 that belongs to the C=C double bond in the same configuration. When I is formed ($\xi \approx 0.9$), the positive

charge is delocalized between C^2 and C^4. The future propene fragment (containing C^4) is still close to the aluminum atom at this stage. At the end of the reaction ($\xi \rightarrow 1.8$), the two fragments are free to move in the microporosity of chabazite. The tert-butylium cation with a large positive charge on the C^2 is closer to the aluminium atom. The charge of C^4 that belongs to the C=C double bond of the propene is reduced at this stage.

In B_2 β-scission, the secondary propenium cation formed in the conventional mechanism (Scheme 1) is highly reactive. Thus, we investigated the mechanism depicted in Figure 4-a by blue moon simulation (SI S12), where spontaneous proton transfer occurs between the propenium cation and the zeolite. In the first part of this profile, from $\xi = -0.70$ to $\xi \approx 0$, isobutene and propenium cation are formed. Most of the C^3-C^4 interaction is lost in this part of process. At this stage, the O^4-H^1 bond is not formed yet, nor the C^7-H^1 bond is broken (Figure 4-b). There is no stationary point on this part of the free energy profile. In the next stage, from $\xi \approx 0$ to 0.75, a proton from a terminal methyl group of the propenium cation is transferred to zeolite. At the TS ($\xi^* \approx 0.20$), the wide distribution of the C^3-C^4 distance indicates that the C^3-C^4 bond is broken and that the two fragments do not interact strongly any more. Concomitantly, the position of the atom H^1 is essentially fixed by strong interactions with O^4 and C^7 atoms (Figure 4-b). Thus the TS of the overall process does not correspond to the β-scission itself but rather to the proton transfer between the highly unstable propenium cation and the zeolite. This differs from the B_1 mechanism. The corresponding free energie of activation is 84.4 ± 5.3 kJ/mol. In contrast to the B_1 reaction, no new reaction mechanism was identified in a short TPS simulation with 100 trial moves, starting from a TS of B_2.

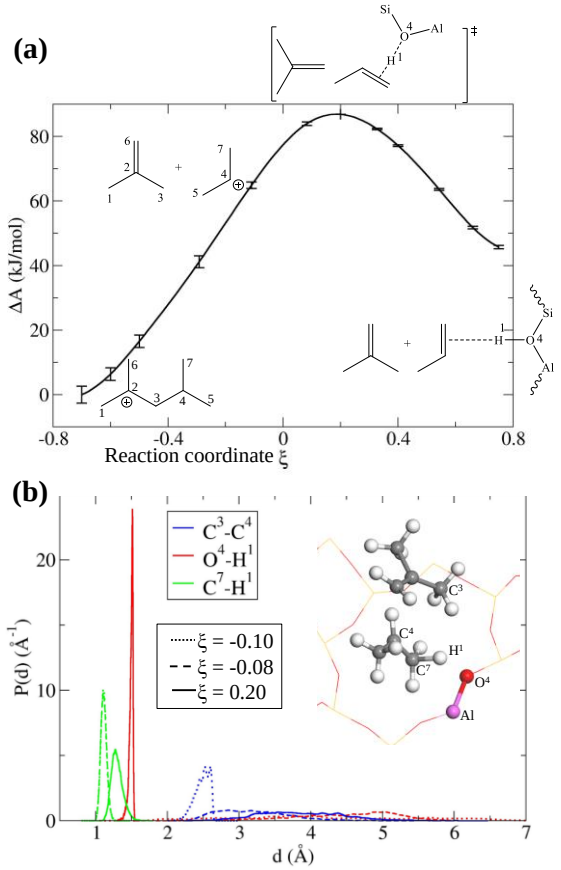

Figure 4. (a) Free energy profile computed using the blue moon ensemble approach for the type B_2 β-scission of 2-4-dimethyl-penten-2-ium into isobutene and π-complex of propene. (b) Probability distributions of selected distances involved in three points along ξ the transition state of the type B_2 cracking reaction, determined using MD. The green curves for the C^7-H^1 distributions at ξ=-0.1 and -0.08 are nearly superimposed. Inset: selected structure from the constrained MD simulation of the transition state of the type B_2 cracking reaction.

Again, the free energy barrier obtained for the type B_2 cracking reaction (84.4 ± 5.3 kJ/mol) is lower than the barriers reported previously. In static DFT, a wide range of large barriers were found (from ~90 to more than 170 kJ/mol,[7f,10,15]). In kinetic modeling an energy barrier of 118 kJ/mol for C_{12} cracking in H-BEA was proposed.[6b] Here also, the large difference between these energy values and our free energies may be attributed to entropic contributions induced by the unsuspected nature of the TS which exhibits two fragments with rather large internal degree of freedom.

The barrier found for B_2 is higher than that for type B_1 cracking (by 17 kJ/mol considering an initial tertiary cation and by 24 kJ/mol starting from a π-complex). The nature of TS differs in each case. The barrier predicted in this work for the type B_2 cracking is about 12 kJ/mol higher than the one proposed for the same reaction of C_8 alkenes in H-ZSM-5 in a recent biased MD study of Cnudde et al.[10] This difference may be attributed to the proton transfer of the propenium to zeolite which is not described in this previous study.

Altogether, considering the present results for B_1 and B_2 cracking, combined with previous AIMD works,[9-10] we propose the following ranking in terms of rate constants: A isomerization ≥ A cracking > B isomerization > B_1 cracking > B_2 cracking, which refines

the empirical knowledge[2a] in terms of respective ranking of the B_1 and B_2 β-scission rates. The unprecedented dynamic structural feature of the B_1 β-scission showing a global rotation of the C_7 species in the course of the reaction, shall be sensitive to shape selectivity. Moreover, the internal rotational degree of freedom found for the B_1 TS is at the origin of entropic effects lowering the overall free activation energies with respect to activation energies reported in previous works employing static DFT or kinetic approaches.

Secondary carbenium ions turn out to be very unstable and do not appear as the kinetically relevant intermediates: instead, π-complexes and tertiary carbenium ions are the species that play a role. For cracking reactions, the implication of secondary carbenium ions as virtual reaction products (type B_2) needs to convert into a more stable species (here a propene π-complex), inducing an extra-barrier with respect to the pure β-scission cost. Going beyond DFT to reach chemical accuracy may be needed,[16] as GGA functionals overbind carbenium ions and alkoxides with respect to π-complexes.[17] However, combining this level of calculation with the MD approach is currently prohibitive. Very recent progress made in the development of machine learning AIMD[18] opens new perspectives.

These findings highlight the critical role of AIMD methods to rigorously quantify such subtle effects that appear to be key when addressing hydrocarbon conversions in porous solids, but likely not only. Each time the entropy, other than vibrational, of the reactant/transition state/ product plays a role, advanced AIMD methods are likely to be required to qualify the mechanisms and quantify the relevant rate constants. This work also opens perspectives for the construction of improved predictive kinetic models, thanks to the identification of the relevant reaction intermediates, and integration of AIMD rate constants.

Acknowledgements

HPC resources were used from GENCI-IDRIS (Grant A0060806134), IFPEN (ENER440), and Computing Center of the Slovak Academy of Sciences (projects ITMS 26230120002 and 26210120002) supported by the Research and Development Operational Program (ERDF). TB acknowledges support from the Slovak Research and Development Agency (Contracts No. APVV−15−0105 and No. VEGA-1/0777/19).

Keywords: zeolite • cracking • alkene • carbenium • acidity

[1] G. Egloff, J. C. Morrell, C. L. Thomas, H. S. Bloch, *J. Am. Chem. Soc.* **1939**, *61*, 3571-3580.

[2] a) C. Marcilly, *Acido-Basic Catalysis*, Technip, Paris, **2005**; b) J. Weitkamp, *ChemCatChem* **2012**, *4*, 292-306; c) U. Olsbye, S. Svelle, M. Bjorgen, P. Beato, T. V. Janssens, F. Joensen, S. Bordiga, K. P. Lillerud, *Angew. Chem., Int. Ed* **2012**, *51*, 5810-5831; d) T. Ennaert, J. Van Aelst, J. Dijkmans, R. De Clercq, W. Schutyser, M. Dusselier, D. Verboekend, B. F. Sels, *Chem. Soc. Rev.* **2016**, *45*, 584-611.

[3] a) H. Pichler, H. Schulz, H. O. Reitemeyer, J. Weitkamp, *Erdöl und Kohle - Erdgas - Petrochemie vereinigt mit Brennstoff - Chemie* **1972**, *9*, 494-505; b) Y. V. Kissin, *Catal. Rev.* **2001**, *43*, 85-146.

[4] J. Weitkamp, P. A. Jacobs, J. A. Martens, *Appl. Catal.* **1983**, *8*, 123-141.

[5] a) J. A. Martens, P. A. Jacobs, J. Weitkamp, *Appl. Catal.* **1986**, *20*, 239-281; b) P. Raybaud, A. Patrigeon, H. Toulhoat, *J. Catal.* **2001**, *197*, 98-112.

[6] a) G. G. Martens, G. B. Marin, J. A. Martens, P. A. Jacobs, G. V. Baron, *J. Catal.* **2000**, *195*, 253-267; b) B. D. Vandegehuchte, J. W. Thybaut, A. Martínez, M. A. Arribas, G. B. Marin, *Appl. Catal. A* **2012**, *441-442*, 10-20; c) T. von Aretin, S. Schallmoser, S. Standl, M. Tonigold, J. A. Lercher, O. Hinrichsen, *Ind. Eng. Chem. Res.* **2015**, *54*, 11792-11803.

[7] a) A. M. Rigby, G. J. Kramer, R. A. van Santen, *J. Catal.* **1997**, *170*, 1-10; b) J. P. Hay, A. Redondo, Y. Guo, *Catal. Today* **1999**, *50*, 517-523; c) S. Namuangruk, P. Pantu, J. Limtrakul, *ChemPhysChem* **2005**, *6*, 1333-1339; d) Y.-X. Sun, J. Yang, L.-F. Zhao, J.-X. Dai, H. Sun, *J. Phys. Chem. C* **2010**, *114*, 5975-5984; e) Y. Chu, B. Han, A. Zheng, F. Deng, *J. Phys. Chem. C* **2012**, *116*, 12687-12695; f) M. N. Mazar, S. H. Al Hashimi, M. Cococcioni, A. Bhan, *J. Phys. Chem. C* **2013**, 23609−23620; g) Y.-H. Guo, M. Pu, B.-H. Chen, F. Cao, *Appl. Catal. A* **2013**, *455*, 65-70; h) B. Huang, P. Bai, M. Neurock, R. J. Davis, *Appl. Catal. A* **2017**, *546*, 149-158.

[8] a) V. Van Speybroeck, K. De Wispelaere, J. Van der Mynsbrugge, M. Vandichel, K. Hemelsoet, M. Waroquier, *Chem. Soc. Rev.* **2014**, *43*, 7326-7357; b) T. Bučko, J. Hafner, *J. Catal.* **2015**, *329*, 32-48; c) P. Cnudde, K. De Wispelaere, J. Van der Mynsbrugge, M. Waroquier, V. Van Speybroeck, *J. Catal.* **2017**, *345*, 53-69.

[9] a) J. Rey, P. Raybaud, C. Chizallet, T. Bučko, *ACS Catal.* **2019**, *9*, 9813-9828; b) J. Rey, A. Gomez, P. Raybaud, C. Chizallet, T. Bučko, *J. Catal.* **2019**, *373*, 361-373.

[10] P. Cnudde, K. De Wispelaere, L. Vanduyfhuys, R. Demuynck, J. Van der Mynsbrugge, M. Waroquier, V. Van Speybroeck, *ACS Catal.* **2018**, *8*, 9579-9595.

[11] P. S. F. Mendes, C. Chizallet, J. Pérez-Pellitero, P. Raybaud, J. M. Silva, M. F. Ribeiro, A. Daudin, C. Bouchy, *Catal. Sci. Technol.* **2019**, *9*, 5368-5382.

[12] a) C. Dellago, P. G. Bolhuis, P. L. Geissler, in *Adv. Chem. Phys.*, John Wiley & Sons, Inc., **2003**, pp. 1-78; b) T. Bučko, L. Benco, J. Hafner, J. G. Ángyán, *J. Catal.* **2011**, *279*, 220-228.

[13] B. Silvi, A. Savin, *Nature* **1994**, *371*, 683-686.

[14] a) P. Bultinck, C. van Alsenoy, P. W. Ayers, R. Carbó-Dorca, *J. Chem. Phys.* **2007**, *126*, 144111; b) T. Bučko, S. Lebègue, J. Hafner, J. G. Ángyán, *J. Chem. Theory Comput.* **2013**, *9*, 4293-4299.

[15] C.-M. Wang, Y.-D. Wang, Z.-K. Xie, *J. Catal.* **2013**, *301*, 8-19.
[16] a) C. Tuma, T. Kerber, J. Sauer, *Angew. Chem. Int. Ed.* **2010**, *49*, 4678-4680; b) G. Piccini, M. Alessio, J. Sauer, *Angew. Chem. Int. Ed.* **2016**, *55*, 5235-5237.
[17] Q. Ren, M. Rybicki, J. Sauer, *J. Phys. Chem. C* **2020**, *124*, 10067-10078.
[18] a) R. Jinnouchi, J. Lahnsteiner, F. Karsai, G. Kresse, M. Bokdam, *Phys. Rev. Lett.* **2019**, *122*, 225701; b) B. Chehaibou, M. Badawi, T. Bucko, T. Bazhirov, D. Rocca, *J. Chem. Theory Comput.* **2019**, *15*, 6333-6342.